

Neuromorphic FPGA Design for Digital Signal Processing

Justin London

*Dept. of Electrical Engineering and Computer Science
University of North Dakota
Grand Forks, North Dakota
justin.london@und.edu*

Abstract—In this paper, the foundations of neuromorphic computing, spiking neural networks (SNNs) and memristors, are analyzed and discussed. Neuromorphic computing is then applied to FPGA design for digital signal processing (DSP). Finite impulse response (FIR) and infinite impulse response (IIR) filters are implemented with and without neuromorphic computing in Vivado using Verilog HDL. The results suggest that neuromorphic computing can provide low-latency and synaptic plasticity thereby enabling continuous on-chip learning. Due to their parallel and event-driven nature, neuromorphic computing can reduce power consumption by eliminating von Neumann bottlenecks and improve efficiency, but at the cost of reduced numeric precision.

I. INTRODUCTION

Neuromorphic computing enables continuous on-chip learning and adaptation to new information without requiring extensive retraining using memristors. Memristors or resistive switches are passive, nonlinear circuit elements with variable nonvolatile resistance states, similar to biological synapses. They are compatible with CMOS technology. Memristor-based Spiking Neural Networks (SNNs) with temporal spike encoding enable ultra-low-energy computation, making them ideal for battery-powered intelligent devices [1, 21]. SNNs are building blocks for neuromorphic computing. In SNN circuit implementations, memristors enable the co-location of computation and memory, thus alleviating the memory bottleneck problem, a major impediment to data-intensive artificial neural network (ANN) workloads. They can be defined as the underlying

computations performed by neuromorphic physical systems which carry out robust and efficient neural computation using hardware implementations that operate in physical time. Typically, they are event- or data-driven, and typically they employ low-power, massively parallel hybrid analog, digital or mixed VLSI circuits, and they operate using similar physics of computation used by the nervous system [12].

In particular, neuromorphic computing focuses on hardware systems that mimic the structure and function of the biological brain, typically involving neural networks and spiking neurons. Neuromorphic FPGAs use CMOS devices and circuits to emulate neurons and synapses, and process data as spikes instead of continuous inputs [11]. Memristors and SNNs have been used in deep learning neuromorphic FPGA designs [8]. The main components of a memristive SNN include a temporal spike encoder, dual switches, a memristive crossbar (MC), Leaky Integrate-and-Fire (LIF) neurons, and various proposed control modules such as the lateral inhibition circuit (LIC), synapse control circuit (SCC), dual switch control circuit (DCC), and update control circuit (UCC) [20]

Spikes that are distributed in space can be parallel processed, and those that are triggered across different times can be serialized. In the absence of spiking events, less memory access are required, though computing spike-based workloads still benefit from parallel processing. The sparsity of

spike-based activations results in large sub-blocks of tensors remaining inactive in GPUs, which are not effectively optimized for sparsity, nor can they be reprogrammed to be so [10]. von Neumann architecture prevalent in CPU and GPU processing enables data transfers between the processing unit and memory unit can lead to high power dissipation. FPGAs provide highly parallel processing, high flexibility, and are reprogrammable; and therefore are suitable for spiking neural networks used in neuromorphic computing which can be applied to digital signal processing and filtering.

Finite impulse response (FIR) filters are non-recursive (feed-forward only) and offer linear phase characteristics, a major advantage in many DSP applications. Infinite impulse response (IIR) filters are recursive (using feedback paths) and can achieve sharper frequency responses with fewer resources than equivalent FIR filters [25]. FPGAs are well-suited for DSP applications due to their inherent parallelism and dedicated DSP slices (e.g., Xilinx DSP48E elements) that efficiently perform multiply-accumulate (MAC) operations. Verilog can be used to describe the digital logic for these filters. Since, memristors can perform both data storage and computation within the same physical location (in-memory computing), overcoming the “von Neumann bottleneck” that limits the speed and power efficiency of traditional computer architectures, they are particularly useful for accelerating the multiply-and-accumulate (MAC) operations central to many DSP and AI tasks.

This study will implement digital signal processing FIR and IIR low-pass filters using Verilog HDL for FPGA design/synthesis and LTSpice for circuit simulation. MUX-based multipliers, adders, or distributed arithmetic techniques to optimize for area, power, and speed will be used in their design. To improve efficiency and speed, multiplexer-based truncated multipliers and approximate adders can also be used in their design. [3] The FIR and IIR will then be redesigned to make them neuromorphic. This can involve replacing the output stage with a SNN such as a leaky integrate-and-fire neuron model. The filter’s output can serve as the synaptic input current

to this neuron. Instead of direct digital convolution, the filter can be implemented as a network of digital spiking neurons, where data is represented by spike times or rates. The data-in and data-out would then represent spike events or encoded signals. Neurons only process information when they receive a spike. This can dramatically reduce power consumption compared to traditional DSP filters that constantly perform computations using sequential logic and shift registers to store previous inputs and outputs needed.

Standard FIR and IIR filters can be incorporated as neuromorphic components in an FPGA design. We seek to first design standard FIR and IIR filters for an FPGA using Verilog. A neuromorphic-inspired DSP filter architecture using SNNs, that mimics the structure of neural networks to perform filtering tasks, which may be more efficient in processing than traditional FIR/IIR designs, will then be implemented. The objective of this work is to show how neuromorphic processing can improve the efficiency and processing of DSP filters in FPGAs. Traditional DSP uses standard multipliers. Neuromorphic memristor-based designs might use highly scalable parallel spike-based digital multipliers or other novel arithmetic units to reduce power and area consumption.

In contrast to standard DSP filters, neuromorphic filters can use adaptive tap coefficients often incorporate on-chip learning, meaning the COEFF values change dynamically using algorithms like LMS (Least Mean Squares), requiring the coefficients to be stored in re-writable RAM instead of ROM or parameters. SNNs can achieve high energy efficiency with lower storage requirements, as they use sparse, binary (0-1) signals instead of real-valued activations and feature maps. Since some SNN-based filters can be designed with self-adaptive time windows, they can in principle be more robust to handling noise compared to traditional filters.

Unlike traditional processors that require constant clock cycles and data movement, neuromorphic chips compute only when a signal is received, process data closer to where it is stored (in-memory

computing), and use analog computation to perform mathematical operations more efficiently. Thus, neuromorphic computing can improve DSP performance by leveraging its event-driven, massively parallel, and memory-centric architecture, which leads to lower power consumption and higher efficiency for certain tasks like sensor processing and inference.

The FIR And IIR algorithms use signed integers to represent Q-format fixed-point numbers with integer and fractional bits. Default parameters ($DATA_W = 24$, $FRAC \approx 16$) give a good mid-ground. One must choose FRAC consistently across signals (coefficients, data, thresholds). Memristors can be used in DSP and neural computing for non-volatile memory as they retain their resistance states (memorpy) without power, enabling energy-efficient in-memory computing and mimicking biological synaptic plasticity.

This paper is organized as follows. In section II, the methodology used is detailed. The methodology covers a background discussion of leaky integrate-and-fire models, FIR filters, and IIR Biquad filters, respectively. In III, the details of memristors, the foundational elements for neuromorphic computing, are discussed. Time registers and operational logic as well as time-domain modules used in DSP are provided. In section section IV, FPGA design for DSP is covered. In section V, the results of the simulation are provided and analyzed. Finally, section VI concludes.

II. METHODOLOGY

In this study, Xilinx Vivado/Verilog HDL and LTSpice are used to implement and simulate waveforms and schematics for FIR filters, IIR filters, and memristors/neuromorphic filter models for digital signal processing. We use a leak integrate-and-fire neuron (LIF) model. A leaky integrate-and-fire neuron models a neuron's behavior by integrating input currents and, when the membrane potential crosses a threshold, "firing" a spike and resetting. The "leaky" part comes from an exponential decay of the membrane potential toward a resting potential, similar to an RC circuit. Incoming signals from other

neurons are modeled as current pulses that add to the neuron's total membrane potential where the membrane has leaky potential. At the same time, the membrane potential naturally "leaks" back towards a resting potential. The fundamental equation for the LIF that describes how a neuron's membrane potential changes over time is:

$$\tau \frac{dV}{dt} = -(V(t) - V_{rest}) + RI_{in}(t) \quad (1)$$

where $V(t)$ is the membrane potential, τ is the membrane time constant, V_{rest} is the resting potential, R is the membrane resistance, and $I_{in}(t)$ is the input current. Let $C = \frac{\tau}{R}$ be the equivalent capacitance of the membrane. so that the LIF neuron can be written as:

$$I_{in}(t) = \frac{V(t) - V_{rest}}{R} + C \frac{dV}{dt} \quad (2)$$

In FPGAs, this continuous function can be discretized using Euler integration resulting in hardware-friendly difference equations. There are various spike neural network models and variations such as the adaptive exponential integrate and fire (AdEx) model, Hodgkin-Huxley, and Izhikevich model [10] Figure 1 compares the neuron models:

Name	Formula	Neuron Models	
		Bio. plausibility	Complexity
Integrate-and-Fire (IF)	$\frac{dv}{dt} = RI$	V. Low	5 FLOPs
Leaky IF (LIF)	$\frac{dv}{dt} = -(v - V_{rest}) + RI$	Low	10 FLOPs
Izhikevich (IZH)	$\begin{cases} \frac{dv}{dt} = 0.04v^2 + 5v + 140 - u + I \\ \frac{du}{dt} = a(bv - u) \end{cases}$	Low	60 FLOPs
FitzHugh-Nagumo (FHN)	$\begin{cases} \frac{dv}{dt} = v - \frac{v^3}{3} - w + I \\ \frac{dw}{dt} = 0.08(v - 0.7 - 0.8w) \end{cases}$	Medium	100 FLOPs
Adaptive IF (AdEx)	$\begin{cases} \frac{dv}{dt} = \frac{-g(v - E_L) + g_L \Delta t \exp(-\frac{v - E_L}{\tau_f}) - w + I}{C} \\ \frac{dw}{dt} = a(v - E_L) - w \end{cases}$	Medium	200 FLOPs
Hodgkin-Huxley (HH)	$\begin{cases} \frac{dn}{dt} = \alpha_n(U)(1 - n) - \beta_n(U)n \\ \frac{dm}{dt} = \alpha_m(U)(1 - m) - \beta_m(U)m \\ \frac{dh}{dt} = \alpha_h(U)(1 - h) - \beta_h(U)h \end{cases}$	High	1200 FLOPs

Figure 1: Comparison of Neuron Models. [22]

Figure 2 (left) illustrates the behavior of a LIF spiking neuron. The spiking neuron receives spikes from several inputs, processes them, and generates output spikes from its output node. The temporal evolution of the neuron state while it receives input spikes is shown on the right. When the threshold is reached, it generates and output spike.

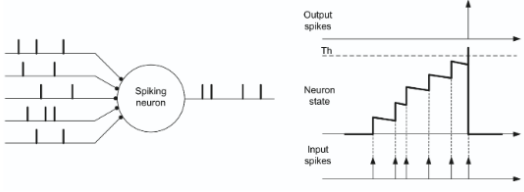


Figure 2: (left) Leaky integrate-and-fire spiking neuron; (right) temporal evolution of the neuron state while it receives input spikes. [4]

Figure 3 illustrates an RC leaky-and-integrate neuron hardware implementation.

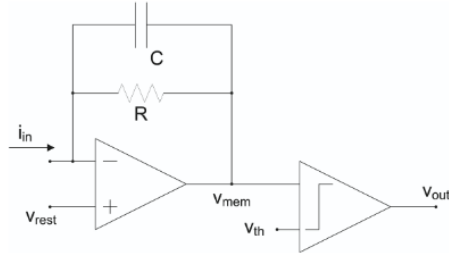


Figure 3: RC LIF neuron implementation. [4]

The neuron's decay is governed by a membrane time constant (τ), which determines how quickly the potential drops. If the integrated potential reaches a specific threshold voltage, the neuron "fires" an action potential (a spike). Resetting: Immediately after firing, the neuron's membrane potential is reset to a lower value (often the resting potential). A brief, absolute refractory period follows the spike during which the neuron cannot fire again, though this is often handled simply by the reset mechanism. A higher input current leads to a faster rise to the threshold, resulting in a higher firing rate.

Spike timing-dependent plasticity (STDP) is a common learning rule implemented on-chip. The synaptic weight updates depend on the relative timing of pre- and post-synaptic spikes. The mathematical expression typically involves adding or subtracting a value from the synaptic weight based on the time difference, often using simple mask-and-accumulate operations instead of complex multiply-

and-accumulate (MAC) as in traditional AI. Hardware arithmetic implementations use fixed-point arithmetic, reconfigurable multipliers, and spike encoding.

Most FPGA-based neuromorphic systems use fixed-point number representation (e.g., 16-bit or 18-bit) for weights and membrane potentials because it uses fewer hardware resources (e.g., look-up tables (LUTs) and flip-flops (FFs)) and less power compared to floating-point. FPGAs have embedded hardware multipliers (DSPs), but their use is optimized to handle the varied precision requirements of neuromorphic workloads, sometimes employing approximate computing techniques to balance accuracy and resource usage. Information is primarily conveyed through binary spikes (event-driven), not continuous values, which simplifies the math to "mask-and-accumulate" or addition operations when a spike arrives.

A. FIR Filters

An FIR filter of length M with input $x(n)$ and output $y(n)$:

$$y(n) = \sum_{k=0}^{M-1} b_k x(n-k) \quad (3)$$

Alternatively, the output sequence can be expressed as a sequence as the convolution of the unit sample response $h(n)$ of the system with the input signal yielding

$$y(n) = \sum_{k=0}^{M-1} h(k) x(n-k) \quad (4)$$

where $b_k = h(k)$. The filter can be characterized by its system function

$$H(z) = \sum_{k=0}^{M-1} h(k) z^{-k} \quad (5)$$

where z^{-k} is the lag of degree k

The frequency response is $H(e^{j\omega}) = \sum_{k=0}^{N-1} h[k] e^{-j\omega k}$ where $h[k]$ are the filter coefficients. ω is the frequency in radians per sample (ranging from 0 to π radians, where π

is the Nyquist frequency.) To compute the gain of an FIR filter, we use the formula for the frequency response, $H(\omega) = \sum_{k=0}^{N-1} h[k]e^{-j\omega k}$, where $h[k]$ are the filter coefficients, N is the filter length, and ω is the frequency. The magnitude of this complex value, $|H(\omega)|$, is the linear gain at that specific frequency. For a specific case like the DC gain (at 0 Hz), the gain is simply the sum of all coefficients: $G_{DC} = \sum_{k=0}^{N-1} h[k]$. To express the gain in decibels, we use the formula: $Gain_{dB} = 20 \log_{10}(|H(\omega)|)$.

FIR Digital Signal Processors (DSPs) primarily use dedicated multiplier-accumulate (MAC) units, along with adders, subtractors, registers (for pipelining and delay lines), and multiplexers. These are often combined into specialized, highly efficient "DSP blocks" within FPGAs or as hardwired components in standalone DSP chip. Multipliers are often 48-bit or 64-bit registers that perform a series of multiply-add operations (Multiply-Accumulate, or MAC units) which is central to FIR filter operation. Pipelining registers/shift registers are essential for the tap-delay lines in FIR filters. The input data is passed through a series of registers to create the necessary delays for each tap, allowing for high performance through pipelining.

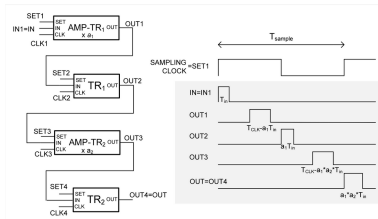


Figure 4: (a) Time-mode z^{-1} multiplier circuit, (b) pulses timing diagram. [18]

In DSP, a time-mode z^{-1} operator multiplier, where $T_{in}(k)z^{-1} = T_{out}(k) = T_{in}(k-1)$, is required to produce an output pulse with pulse T_{out} width equal to $a \cdot T_{in}$, where T_{in} is the input pulse and a is the multiplication coefficient, and the output pulses will be synchronized with the sampling signal and delayed by one clock cycle. Figure 4 shows the time-mode z^{-1} multiplier circuit and timing pulses.

A time-mode z^{-1} multiplier is realized using the combination of two AMP-TR and two TR circuit series as shown in Figure 5.

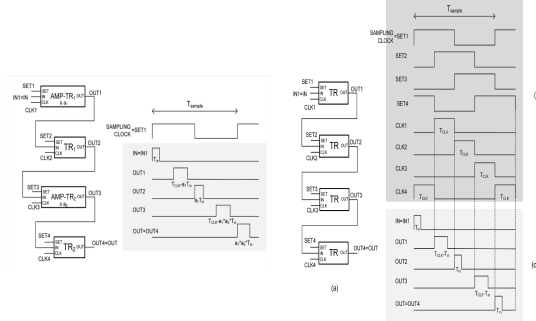


Figure 5: (left) (a) Time-mode z^{-1} multiplier circuit; (b) pulse timing diagram; (right) (a) Time-domain z^{-1} circuit, (b) clocks timing diagram, and (c) pulses timing diagram [18]

B. IIR Biquad

The general formula for an infinite impulse response (IIR) filter is the difference equation:

$$y[n] = \sum_{k=0}^M b_k x[n - ki] - \sum_{k=1}^N a_k y[n - k] \quad (6)$$

representing the current output $y[n]$ as a weighted sum of current/past inputs and past outputs using feedforward (b) and feedback (a) coefficients, or its transfer function:

$$H(z) = \frac{B(z)}{A(z)} = \frac{\sum_{k=0}^M b_k z^k}{1 + \sum_{k=1}^N a_k z^{-k}} \quad (7)$$

The term "biquad" is short for bi-quadratic and is a common name for a two-pole, two-zero digital filter. The transfer function of the biquad can be defined as:

$$H(z) = g \frac{1 + \beta_1 z^{-1} + \beta_2 z^{-2}}{1 + a_1 z^{-1} + a_2 z^{-2}} \quad (8)$$

C. Butterworth Filter

Consider a 2nd order Butterworth (Sallen-Key) low pass filter shown in Figure 6.

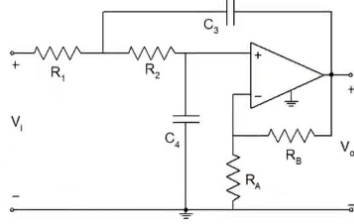


Figure 6: 2nd order filter

Assume $\alpha = 7$ and $\beta = 6$. The DC gain $K = \frac{4+\alpha}{2} = \frac{4+7}{2} = 5.5$. The cut-off frequency $= f_c = \frac{4+\beta}{2} = \frac{4+6}{2} = 5\text{ KHz}$. Let $f_c = \frac{1}{2\pi\sqrt{R_1R_2C_1C_2}}$ be the cut-off frequency and assume $R = R_1 = R_2$ and $C = C_1 = C_2 = 15\text{nF}$ yielding $f_c = \frac{1}{2\pi RC}$ so that $R = \frac{1}{2\pi f_c C} = \frac{1}{2\pi(5\text{kHz})(15\text{nF})} = 2.2\text{k}\Omega$. The transfer function is

$$\frac{V_o(s)}{V_i(s)} = \frac{K \frac{1}{R_1 R_2 C_3 C_4}}{s^2 + s\left(\frac{1}{R_1 C_3} + \frac{1}{R_2 C_3} + \frac{1}{R_2 C_4} - \frac{K}{R_2 C_4}\right) + \frac{1}{R_1 R_2 C_3 C_4}}$$

or

$$\frac{K \frac{1}{R^2 C^2}}{s^2 + s\left(\frac{1}{RC} + \frac{1}{RC} + \frac{1}{RC} - \frac{K}{RC}\right) + \frac{1}{R^2 C^2}}$$

Plugging in the values yields

$$\frac{V_o(s)}{V_i(s)} = \frac{5.05 \times 10^9}{s^2 - 75757.7s + 9.2 \times 10^8} \quad (9)$$

where $K = 1 + \frac{R_A}{R_B}$. If $R_A = 1\text{k}\Omega$, then $R_B = 4.5\text{k}\Omega$. We show the BW low pass filter circuit and simulation in LTSpice as shown in Figure 7 and 8, respectively.

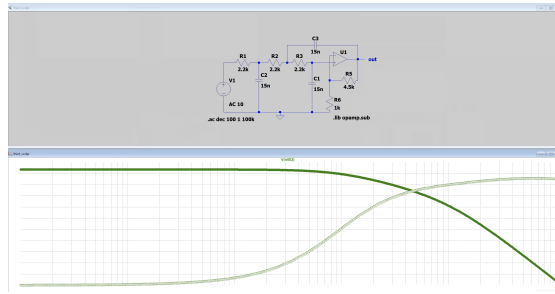


Figure 7: BW Circuit in LTSpice

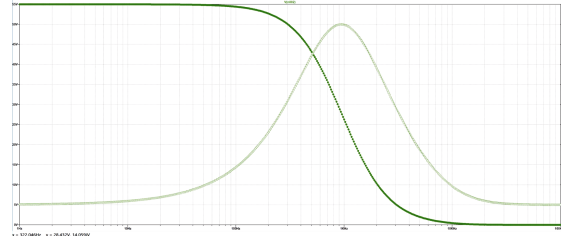


Figure 8: LTSpice Simulation of BW Filter

D. High Passfilter

Figure 9 illustrates an LTSpice simulation for a third-order active high pass filter which uses two differential op amplifiers.

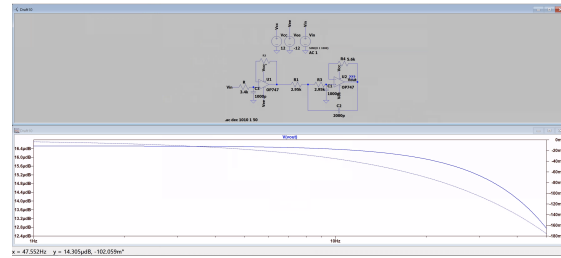


Figure 9: Highpass Filter

Figure 10 illustrates an LTSpice simulation for a passive bandpass filter:

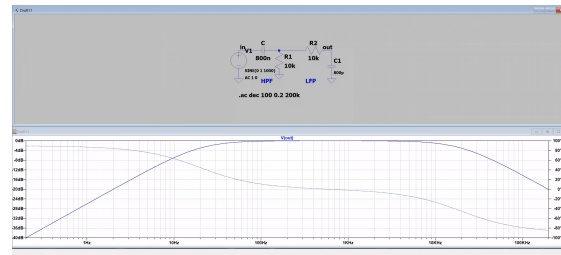


Figure 10: Bandpass Filter

III. MEMRISTORS

A memristor-based neuron, two-terminal/electrode switches with variable conductance, has input signals x_1, \dots, x_n that are directed to synapses based on memristors,

with corresponding weights w_1, \dots, w_N [16]. The change in the respective synaptic weight is realized by alteration of the corresponding memristance with externally applied voltage or current pulses. They are have low power consumption, high switching speed, and good compatibility with complementary metal oxide semiconductor (CMOS) technology [15]. Figure 11 illustrates a schematic of a memristor. The top electrode is denoted te and the bottom electrode is be . A sinusoidal voltage source supplies the memristor equivalent circuit. The memristor current is modeled by the voltage-controlled current source G_1 . The current of this dependent source is the memristor current. The additional electrode for measuring the memristor state variable x is denoted Y . The time derivative of the state variable is proportional to the memristor current and is expressed by the dependent, voltage-controlled current source $G_2 \equiv G_Y$. The capacitor load is used for integrating the current proportional to the time derivative of the memristor state variable x . The corresponding

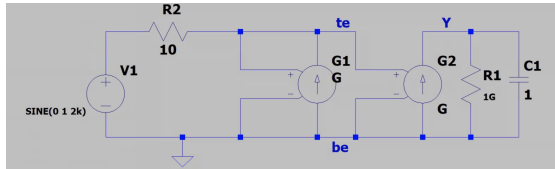


Figure 11: Memristor Circuit

LTS spice netlist code for memristor model denoted $K1$ is:

```

1 .subckt K1 te be Y
2 .params ron = 100 roff = 16e3 k = 10e3 C1 = 1
3 C1 Y be IC = 0.3
4 R2 Y be 1G
5 Gy 0 Y value = (k V(te,be) (1/(ron(V(Y)) + roff(1 - V(Y))))(4V(Y)(1 - V(Y)(1 - V(Y))))}
6 G1 te be value = V(te,be) ((1/(ron(V(Y)) + roff(1 - V(Y)))))
7 End K1

```

Most memristors are based on transition metal oxides such as titanium dioxide, hafnium dioxide, and tantalum oxide. Numerous titanium dioxide memristor nanostructure models have been proposed including Strukov-Williams, Joglekar-Biolek, Ascoli-Corinto, and Lehtonen-Laiho [15]. Memristive elements exhibit hysteresis relationship between voltage and current. Figure 12(a) illustrates the memristor

nanostructure representing the metallic contacts (top electrode nad bottom electrode), the doped and un-doped layers of the memristor. Figure 12(b) shows an equivalent circuit representing the resistances of the doped and the un-doped regions connected in series.

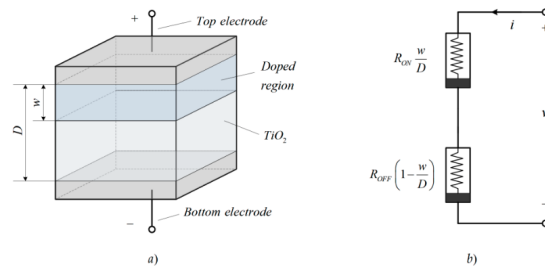


Figure 12: (a) Memristor nanostructure and (b) equivalent electric circuit. [15]

Memristors with diffusive dynamics are well suited to mimick the behavior of synapses as they can be scaled down to feature sizes below 10 nm, can retain memory states for years, switch with nanosecond timescales, and undergo spike-based learning in real time under biologically inspired learning rules as spike-time-dependent plasticity (STDP) [21]. The characteristic I-V equations of a memristive element can be approximated by:

$$i_{MR} = G(w, v_{MR})v_{MR} \quad (10)$$

$$dw/dt = f_{MR}(w, v_{MR}) \quad (11)$$

where i_{MR} and v_{MR} are the current voltage drop at the terminal devices, respectively where

$$f_{MR} = \begin{cases} I_0 \text{sign}(v_{MR}) (e^{|v_{MR}|/v_0} - e^{v_{TH}/v_0}) & \text{if } |v_{MR}| > v_{TH} \\ 0 \text{ otherwise} & \end{cases} \quad (12)$$

$G(w, v_{MR})$ is the conductance of the device that changes as function of the applied voltage (assuming a voltage or flux controlled device model), and w is some physical parametric characteristic whose change is typically governed by a nonlinear function f_{MR} of the applied voltage including a threshold barrier [4]. They are typically binary

devices switching between high resistance state and low resistance state.

In hardware, a learned neural approximator can approximate the filter response with fewer dedicated fixed filter taps (fewer multipliers), and in memristor crossbar implementations the MAC is inherent in Ohm's law (vectors multiplied by conductances and summed in analog) — potentially much lower area and power than digital MAC arrays. The trade-offs: approximation error vs resource/power savings. Figure 13 shows the structure of a memristor neural network and 13(b) shows a schematic of a memristor-based synapse. A schematic of a passive

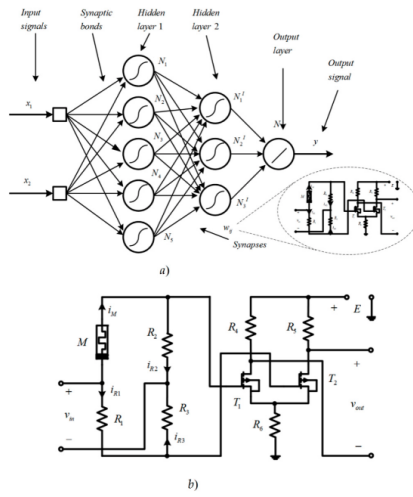


Figure 13: (a) Memristor neural network and (b) memristor-based synapse. [15]

memristor memory crossbar is shown in Figure 14(a) and its equivalent circuit is shown in Figure 14(b). The memristor memory crossbar schematic in LTSpice is shown in Figure 14(c).

A. Time Registers and Operational Logic

The time register (TR) or shift register is a sequence of flip flops that stores bits and shifts them alone one position with each clock pulse, creating a time delay or performing serial-to-parallel/parallel-to-serial conversion, acting as temporary data storage synchronized by a clock. Figure 15 shows the time

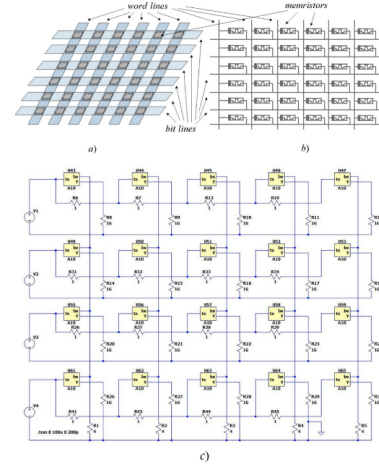


Figure 14: (a) Memristor memory crossbar; (b) equivalent circuit; (c) LTSpice schematic. [15]

register and its symbol. If $SET = 0$, transistor M_1 , a PMOS, is turned on, and the capacitor voltage is set to the supply voltage V_D . The capacitor discharges when the transistor M_2 , an NMOS, is ON, which is controlled by an OR gate [18].

Figure 15 is a time diagram of a time register that tracks the synchronization procedure. The SET signal's time interval T_{CLK} is a pulse with a fixed pulse width and a 25% duty cycle. When both IN and CLK are 0, then the capacitor voltage remains constant. The larger the pulse width T_{in} of the IN signal, the more discharging time due to T_{in} appeared, considering that the discharging time due to CLK stays the same. The output is a pulse with a width equal to $T_{CLK} - T_{in}$, allowing the value of T_{in} to be stored while the output pulse is synchronized with the CLK signal.

The circuit can store the time interval of an input pulse and amplify the pulse width by a gain factor. The new circuit is a time amplifier and is shown on the left in Figure 16. Following Felouris et al. [18], in this configuration, the operation of the OR gate is performed by the two-transistor branches $M_{a1}-M_{b1}$ and $M_{a2}-M_{b2}$. Transistors M_{a1} and M_{a2} have the same aspect ratio acting as switches. The aspect ratios of M_{b1} , M_{b2} are different, featuring a different

discharging slope. Assuming that the channel widths of M_{b2} and M_{b1} are $W_{b,2}$ and $W_{b,1}$, respectively, while both transistors have the same channel length. Then, intuitively, using Figure 5(c), the discharging slope between T_{in} and T_{CLK} will be different. The discharging slope in that corresponds to T_{in} will be given by

$$slope_{in} = a \cdot slope_{clk} \quad (13)$$

where a is the time gain and is given by

$$a = \frac{W_{b,2}}{W_{b,1}} \quad (14)$$

and $slope_{clk}$ is the discharging reference slope caused by T_{CLK} . Therefore, the output pulse width will be equal to

$$T_{OUT} = T_{CLK} - \frac{W_{b,2}}{W_{b,1}} T_{in} \quad (15)$$

The right side of Figure 16 shows a time adder circuit which is based on the time register. A time adder simply adds the pulse widths $T_{in,1}, T_{in,2}, \dots, T_{in,n}$ of n number input pulses. Transistors $M_{b,1}, M_{b,2}, \dots, M_{b,n}, M_{b,n+1}$ have the same aspect ratio [18]. Therefore, the discharging slope caused by $T_{in,1}, T_{in,2}, \dots, T_{in,n}$ will be given by

$$slope_{in,1, in,2, \dots, in,n} = slope_{in,1} + slope_{in,2} + \dots + slope_{in,n} \quad (16)$$

and the output pulse width will be

$$T_{OUT} = T_{CLK} - T_{in,1} - T_{in,2} - \dots - T_{in,n} \quad (17)$$

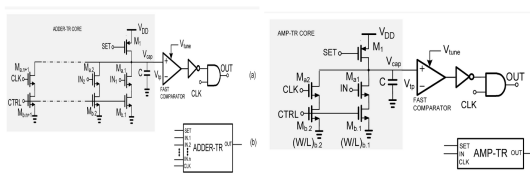


Figure 16: (left) Time amplifier on time register circuit and symbol (ADDER TR); (right) time adder based on time register and symbol (AMP TR) [18]

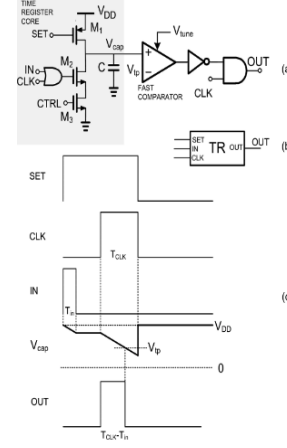


Figure 15: (a) Time register circuit; (b) symbol; and (c) timing diagram [18]

B. Time-Domain Modules

DSP uses time lag/delay operations using a time mode z^{-1} multiplier is to produce an output pulse with pulse T_{out} width equal to aT_{in} where T_{in} is the input pulse and a is the multiplication coefficient, and the output pulses will be synchronized with the sampling signal and delayed by one clock cycle. A proposed z^{-1} circuit is shown on the left in Figure 5 and the waveforms are shown on the right. A combination of four TR circuits in series realizes a z^{-1} circuit. The SAMPLING CLOCK signal is assumed to be the SET1 signal of the TR1 circuit, and the input signal IN is equal to the input IN1 of TR1, while the final output signal OUT is the output of OUT4 of TR4 [18].

To be synchronized with the SET2 pulse, the OUT1 pulse is generated at the rising edge of CLK1. After that, the OUT1 was used as the TR's input. OUT2 is synchronized with CLK2, and $T_{OUT2} = T_{CLK} - T_{OUT1} = T_{CLK} - (T_{CLK} + T_{in}) = T_{in}$

IV. FPGA DESIGN FOR DSP

IBM's TrueNorth Chip [2] and Intel's Loihi [7] are ASIC chips with neuromorphic architectures. The TrueNorth core comprises five components:

neuron block, core sram, router, scheduler, and token controller [23]. A single TrueNorth chip comprises 4,096 neurosynaptic cores. Valancius et. al. [23] prototypes the TrueNorth architecture as a reference for a parameterized and configurable emulation platform for FPGA neuromorphic architecture on the Xilinx Zynq UltraScale+ MPSoC. They validate the functionality of their emulation environment using the MNIST dataset and vector matrix multiplication case studies and demonstrate increased computational efficiency, reduced computing time, and a reduction in resource utilization while maintaining high accuracy. A systematic review of digital neuromorphic architectures (NMAs) implemented on FPGAs is given in [22].

FPGAs provide numerous multiply-accumulate (MAC) functions which are the fundamental building block of DSPs. In contrast, a traditional DSP provides only one to four such MACs. The Virtex-4 family of Xilinx, built on an ASMLB architecture, contains a new element called the DSP48 slice that integrates high performance arithmetic and accumulation unit along with a multiplier. DSP48 slices are cascadable into tiles known as XtremeSDP tiles with two sets. The DSP48 slice comprises four main sections: I/O registers, 18×18 signed multiplier, three input adder/subtractor blocks, and OPMODE multiplexers that support over 40 unique operations at 500 Mhz. For DSP applications, the DSP48 modules would be used on the FPGA hardware. Figure 17 shows a DSP48 tile consisting of two DSP48 slices.

The 18-bit A bus and A bbus are concatenated, with the A bus being the most significant. The X, Y, and Z multiplexers are 48-bit designs. Selecting any of the 36-bit inputs provides a 48-bit sign-extended output. The multiplier outputs two 36-bit partial products, sign extended to 48 bits. The partial products feed the X and Y multipliers. When OPMODE selects the multiplier, both X and Y multiplexers are utilized and the adder/subtractor combines the partial products into a valid multiplier result. The multiply-accumulate path for P is through the Z multiplier. The P feedback through the X multiplexer enables accumulation of P cascade

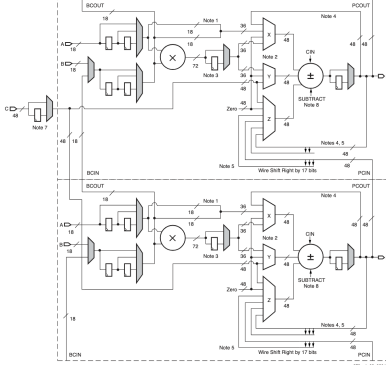


Figure 17: DSP48 tile with two DSP48 slices. [26]

when the multiplier is not used. The grey-color multiplexers in 17 are programmed at configuration time. The shared C register supports multiply-add, wide addition, or rounding. Enabling SUBTRACT implements $Z - (X+Y+CIN)$ at the output of the adder/subtractor [26].

This DSP architecture can be modified with an FPGA-based neuron array design, such as proposed by Cassidy et al. [5] (illustrated in Figure 18), that integrate spiking neuron networks using synapses, a delay mechanism, an accumulator, thresholds, and spike-time-dependent plasticity [13].

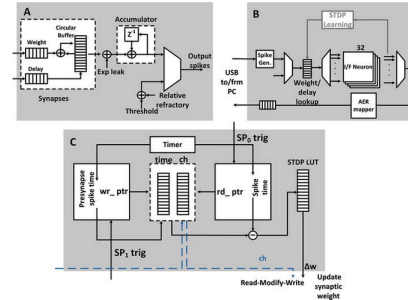


Figure 18: FPGA-based neuron. A: details the the individual neuron architecture; B: shows the overall network architecture including interfaces for spike generation; C: implementation of STDP [5]

Pearson et. al. [19] propose an FPGA-based array processor architecture simulating large networks

with more than a thousand neurons for real-time signal processing. However, the scalability is limited by a bus-based communication protocol. More advanced SNN architectures have been introduced for neuromorphic FPGAs including Optimized Deep Event-driven Spiking Neural Networks (ODESA) [14], Polychronous Spiking Neural Networks (PSNN) [9, 24], and Embedded Multicore Building Blocks for Reconfigurable Architecture Computational Emulation (EMBRACE-FPGA) [17, 6, 12].

ODESA is a multi-layered architecture that employs gradient-free, threshold-based learning algorithm that dynamically adjusts synaptic weights and neuronal thresholds based on local synaptic behavior and a Winner-Takes-All (WTA) mechanism. Each neuron operates in an event-driven manner, processing inputs as discrete binary spikes, significantly reducing power consumption and processing. In PSNNs, spikes from different neurons travel down axons with precise delays, arriving simultaneously at a target neuron and causing it to fire, even though the source neurons fire asynchronously. Instead of employing traditional analog neurons, EMBRACE models these neurons using soft-processors on the FPGA, facilitating a novel approach to neural computation that leverages the reconfigurability of digital systems.

V. RESULTS

We simulate a sinusoidal signal plus Gaussian noise using a signal amplitude $A = 0.6$, a frequency $f = 50$ Hz, a noise amplitude $A_{noise} = 0.05$, and then quantized to fixed point Q15.

$$x[n] = A \sin(2\pi f n) + 2A_{noise}(\text{rnd}\%1000)/1000 - 1$$

where $\text{rnd}\%1000$ is a Gaussian random number generator mod 1000 and n is the time step from [0, 2000]. The signal is simulated in both a training phase and then compared in a testing phase each with 2000 time steps. We implement a classic FIR, classical IIR, neuromorphic FIR, and neuromorphic IIR models. The neuromorphic FIR model is small feedforward NN (single hidden layer) that approximates the linear FIR convolution. We use a classical FIR: direct-form, parameterized taps, fixed-point (WIDTH bits, FRAC fractional bits) and a

classical IIR direct Form II transposed (numerical stability), parameterized order and fixed-point. The neuromorphic IIR uses a small recurrent neural network (Elman-type) that approximates the IIR filtering behavior and implemented with a recurrent vector multiply and activation (\tanh approximated by LUT).

Neuromorphic versions emulate a memristor weight array in logic (weights stored as registers) and include an LMS learning rule inside the module (for online adaptation). The learning rule is only invoked when $\text{train}=1$ and a desired signal is provided by the testbench. We IIR uses Direct Form I biquad (2nd order) with fixed-point coefficients; The neuromorphic IIR uses an adaptive recurrent weight structure with LMS updates for feedback-/feedforward taps. Testbenches provide the same stimulus (sinusoid + noise, impulse, step) to all variants so output comparison is fair. LTSpice netlists implement crossbar sums using memristors and an op amp current summing node. The memristor behavior is a simple physics-inspired behavioral model (suitable for performance testing). Schematics generated in Vivado for the FIR and Biquad IIR models are shown in Figure 19. Schematics for the

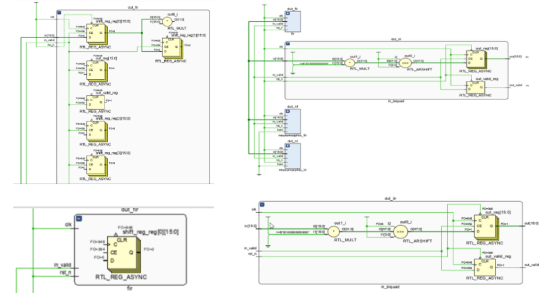


Figure 19: Schematics. (left) FIR and (right) Biquad IIR

neuromorphic FIR and the neuromorphic IIR Biquad are shown in Figure 20. Inputs are tapped samples. In practice, weights are trained offline and loaded into hardware registers (or an on-chip memristor array in LTSpice). It can use fewer multipliers if one quantizes & re-use weights or exploit sparsity. The following table compares the MSE of the models

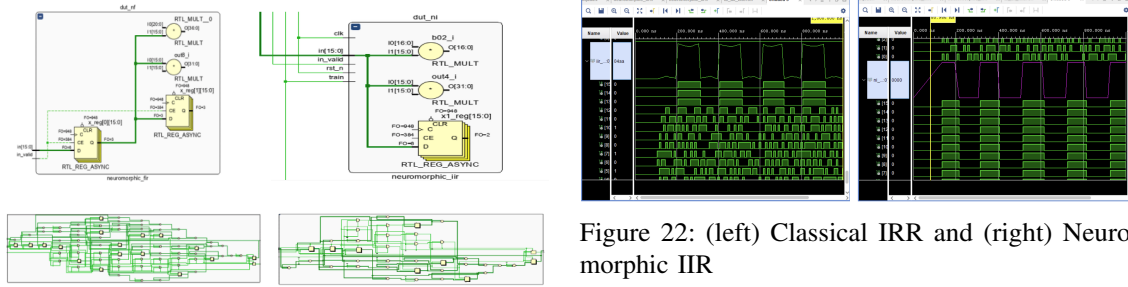


Figure 20: Schematics. (left) neuromorphic FIR and (right) neuromorphic Biquad IIR

relative to the classical FIR golden reference. Thus, the MSE for the classical FIR is 0. Figure 21

Table I: MSE relative to classical FIR golden reference

Model	MSE	Cells	Cell Pins	NetLists
Classical FIR	0.0	173	36	921
Neuromorphic FIR	0.5209	335	53	1544
Classical IIR	0.1374	192	36	1007
Neuromorphic IIR	0.1533	163	53	760

shows the simulated output of the classical FIR (left) and the neuromorphic FIR (right). As shown, the neuromorphic FIR is much more variable than the classical FIR. Neuromorphic Finite Impulse Response (FIR) signals are much more variable than classical FIR signals primarily due to the inherent noise and component variations in the underlying neuromorphic hardware, which often uses analog or mixed-signal circuits to mimic biological processes. Classical digital signal processing (DSP), by contrast, operates on precise numerical values in a highly controlled, deterministic environment.

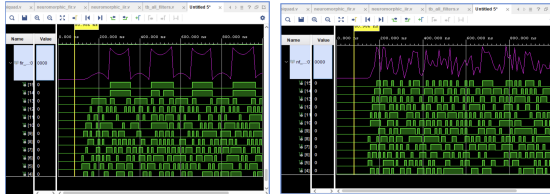


Figure 21: (left) Classical FIR And (right) Neuromorphic FIR

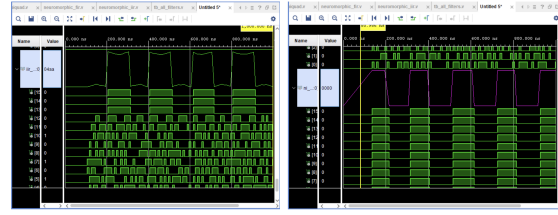


Figure 22: (left) Classical IIR and (right) Neuromorphic IIR

VI. CONCLUSION

Using Vivado and Verilog HDL for FPGA design, FIR and IIR filters using neuromorphic computing were simulated and compared to standard FIR and IIR von Neumann-based filters. Spiking neural networks were used to generate event-based signals. In actual hardware implementation, memristors in DSP48 modules would be used. IIR neuromorphic computing and standard IIR filter have comparable MSEs relative to the FIR golden. The FIR neuromorphic model relative to the standard FIR golden reference has much higher MSE. Though neuromorphic computing may not provide as precision results as standard DSP that uses sequential logic, it does have significant power consumption, efficiency, and cost benefits. Furthermore, the distributed nature of neuromorphic networks makes them inherently more robust to faults or errors. Due to its parallel nature and adaptive learning while integrating processing and memory within the same location, similar to how neurons and synapses work in the brain, neuromorphic computing eliminates the von Neumann bottleneck. Future work will involve research into improving precision for real-time DSP applications and actual FPGA implementation using Xilinx.

REFERENCES

- [1] S. Abreu and J. Pedersen. *Neuromorphic Programming: Emerging Directions for Brain-Inspired Hardware*. 2024. URL: <https://arxiv.org/html/2410.22352v1>.

[2] F. Akopyan et al. “TruthNorth: Design and tool flow of a 65 mw 1 million neuron programmable neurosynaptic chip”. In: *IEEE Transactions on Computer-Aided Design of Integrated Circuits and Systems* 34.10 (2015), pp. 1537–1557.

[3] K. Bali and N. Kumar. “Implementation of FIR Filter Using Multiplexer Based Truncated Multiplier and Approximate Adders”. In: *2025 International Conference on Visual Analytics and Data Visualization (ICVADV), Tirunelveli, India* (2025), pp. 718–723.

[4] L. Camunas-Mesa, B. Linares-Barranco, and T. Serrano-Gotarredona. “Neuromorphic Spiking Neural Networks and Their Memristor-CMOS Hardware Implementations”. In: *Materials* 12 (2019).

[5] A. Cassidy et al. “FPGA based silicon spiking neural array”. In: *IEEE Biomedical Circuits and Systems Conference*. Montreal, Canada, 2007.

[6] S. Cawley et al. “Hardware spiking neural network prototyping and application”. In: *Genetic Programming and Evolvable Machines* 12 (2011), pp. 257–280.

[7] M. Davies et al. “Loihi: A Neuromorphic Manycore Processor with On-Chip Learning”. In: *IEEE Micro* 38.1 (2018).

[8] T. Hong, Y. Kang, and J. Chung. “InSight: An FPGA-Based Neuromorphic Computing System for Deep Neural Networks”. In: *Journal of Low Power Electronic Applications* 10.36 (2020). DOI: [doi:10.3390/jlpea10040036](https://doi.org/10.3390/jlpea10040036).

[9] E. Izhikevich. “Poly-chornization: Computation with spikes”. In: *Neural Computation* 18 (2006), pp. 245–282.

[10] M. Karamimanesh et al. *Spiking Neural Networks on FPGA: A Survey of Methodologies and Recent Advancements*. 2025.

[11] Wei Lu. *Neuromorphic Computing Based on Memristive Materials and Devices*. 2020. URL: <https://www.youtube.com/watch?v=qfBlqCZdG6U&t=261s>.

[12] A. Mehonic et al. *Roadmap to Neuromorphic Computing with Emerging Technologies*. 2024. URL: <https://arxiv.org/abs/2407.02353v1>.

[13] A. Mehrabi and A. van Schaik. “FPGA-Based Spiking Neural Networks”. In: *Recent Advances in Neuromorphic Computing*. IntechOpen, 2024. URL: <https://www.intechopen.com/chapters/1189625>.

[14] A. Mehrabi et al. *Efficient Implementation of a Multi-Layer Gradient-Free Online-Trainable Spiking Neural Network on FPGA*. 2023.

[15] V. Mladenov. “A Unified and Open LTSpice Memristor Model Library”. In: *Electronics* 10 (2021).

[16] V. Mladenov and S. Kirilov. “A Memristor Neural Network Based on Simple Logarithmic-Sigmoidal Transfer Function with MOS Transistors”. In: (2024).

[17] F. Morgan et al. *Exploring the Evolution of NoC-Based Spiking Neural Networks on FPGAs*. 2009. DOI: [10 : 1109 / fpt . 2009 . 5377663](https://doi.org/10.1109/fpt.2009.5377663).

[18] O. Panetas-Felouris and S. Vlassis. “A 3rd-Order FIR Filter Implementation Based on Time-Mode Signal Processing”. In: *Electronics* 11.6 (2022). DOI: <https://doi.org/10.3390/electronics11060902>.

[19] M. Pearson et al. “Implementing Spiking Neural Networks for Real-time Signal-Processing and Control Applications: A Model-Validated FPGA Approach”. In: *IEEE Transactions on Neural Networks* 18.5 (2007), pp. 1472–1478.

[20] S. Prajapati, S. Sur-Kolay, and S. Dutta. *Efficient Memristive Spiking Neural Networks Architecture with Supervised In-Situ STDP Method*. 2025. URL: <https://arxiv.org/html/2507.20998>.

[21] J. Sune. *Memristors for Neuromorphic Circuits and and Artificial Intelligence Applications*. MDPI, 2020.

[22] W. Szczerek and A. Podobas. “A Quarter of a Century of Neuromorphic Architectures on FPGAs - an Overview”. In: *arXiv:2502.20415v3 [cs.AR]* (2025).

[23] S. Valancius et al. “FPGA Based Emulation Environment for Neuromorphic Architectures”. In: *arXiv:2004.06061v1 [cs.ET]* (2020).

- [24] R. Wang et al. “An FPGA Implementation of a polychronous spiking neural network with delay adaption”. In: *Frontiers in Neuroscience* (2013), pp. 7–14.
- [25] R. Woods et al. *FPGA-based Implementation of Signal Processing Systems, 2nd Ed.* Wiley, 2017.
- [26] Xilinx. *DSP: Designing for Optimal Results : High-Performance DSP Using Virtex-4 FPGAs*. Xilinx, 2005. URL: <https://www.xilinx.com/publications/archives/books/dsp.pdf>.